35th Annual International Conference of the IEEE EMBS
Osaka, Japan, 3 - 7 July, 2013

Segmentation of aortic flow in real time magnetic resonance images

Gustavo M. Q. Mendonça[1], and Joao L. A. Carvalho[1]

Abstract— **Real-time spiral phase contrast magnetic resonance imaging (MRI) is capable of non-invasively measuring the stroke volume associated with each individual heartbeat. The quality of these measurements depends on how good the segmentation of the interface between aortic wall and lumen is. Such process is hampered by the low-resolution and low-contrast nature of real-time images. Image segmentation using traditional techniques has proven not robust. This paper presents a novel model-based approach, which is capable of very accurately segmenting aortic flow. Instead of attempting to achieve a millimetrically-accurate segmentation of the wall–lumen interface, the proposed algorithm focuses on separating the aortic flow from neighboring flows. This provides robustness, even when this interface is not visually distinguishable. The proposed segmentation takes real-time MRI one step further towards becoming the non-invasive gold standard for assessment of stroke volume variability.**

I. Introduction

Cardiac output measurement allows evaluating and monitoring the severity of cardiac dysfunctions in patients. However, there is no gold standard for its assessment. Moreover, there is interest in measuring the stroke volume associated with each individual heartbeat, as stroke volume variability provides unique information about autonomic activity, connecting heart rate variability to blood pressure and venous return variabilities [1].

Real-time spiral phase contrast magnetic resonance imaging (MRI) is capable of non-invasively measuring stroke volume variability [2-7]. The quality of these measurements depends on how good the segmentation of the interface between aortic wall and lumen (in cross-section) is. Such process is hampered by the low-resolution and low-contrast nature of the images provided by this method, especially when 3 Tesla (or higher-field) scanners are used, as off-resonance effects are increased. Image segmentation using simple thresholding [2-5] and/or traditional image segmentation techniques — such as denoising, filters, and morphologic operations — has proven not robust [9]. More sophisticated algorithms have proven efficient when applied to certain methods of acquisition, in which contrast and resolution conditions are better [10].

This paper presents a novel, consistent and reliable approach, which is capable of very accurately segmenting aortic flow, for real-time stroke volume measurement. Instead of attempting to achieve a millimetrically-accurate segmentation of the wall–lumen interface, the proposed algorithm focuses on separating the aortic flow from neighboring flows. This provides robustness even when this interface is not visually distinguishable. Segmentation is performed on a model image, constructed by multiplying a high-pass version of the original morphological image by a two-dimensional Gaussian function, centered at the centroid of the aorta. The centroid is estimated for each frame, using a barycenter-based iterative process, which uses template images to highlight both aortic lumen and wall. The proposed segmentation takes real-time spiral phase contrast MRI one step further towards becoming the non-invasive gold standard for assessment of stroke volume variability.

[1]G. M. Q. Mendonça and J. L. A. Carvalho are with the Department of Electrical Engineering, University of Brasilia, Brazil. joaoluiz@pgea.unb.br

II. Materials and methods

A. Image acquisition

Data acquisition was performed using real-time spiral phase contrast MRI, with 57 ms temporal resolution, and 3 mm spatial resolution [2-4]. Slice prescription was performed perpendicular to the ascending aorta. In addition to a morphological image, which maps the T1-weighted spatial distribution of ^{1}H nuclei, phase contrast MRI provides a map of the through-plane velocity of the spins.

Data acquisition was performed on a Signa 3T EXCITE HD MRI scanner (GE Healthcare, Inc.). Seven healthy volunteers participated of the research. The ethics committee of the University of Southern California approved the experimental protocols. All volunteers provided informed consent.

B. Image reconstruction

Image reconstruction and processing were performed in MATLAB (The Mathworks, Inc., Natick, USA). Frame rate was increased by 4-fold using a sliding window reconstruction [8]. This does not improve temporal resolution, but inserts redundant frames, resulting in smaller aortic displacements between two consecutive frames.

C. Image cropping and initialization parameters

The proposed image segmentation algorithm requires two input parameters: an initial estimate of the aortic centroid, (x_o, y_o) (Fig. 1c), and an estimate of the mean aortic radius ($\overline{R}$) (Fig. 1b). These are calculated after the aortic lumen is manually circled (Fig. 1b) on a 10-fold magnified morphological image, obtained by averaging frames from a 5.6-second window (Fig. 1a). The radius vector (Fig. 1b) provides not only the mean radius, but also the maximum axis size direction and eccentricity. After the input parameters are calculated, all frames are cropped around the prescribed region of interest (Fig. 1c). The position and dimension of such region are automatically calculated based on the two parameters described above. The cropped region is large enough to accommodate for intra-beat motion of the aorta during the entire acquisition.

978-1-4577-0216-7/13/$26.00 ©2013 IEEE

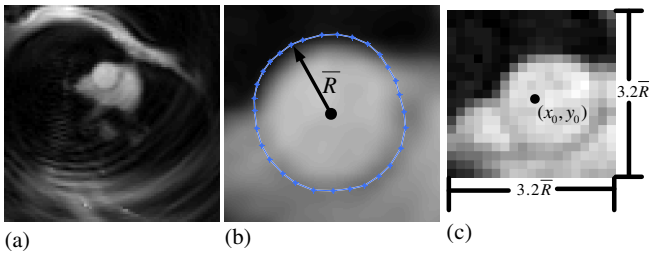

Fig. 1. Image cropping and initialization parameters: (a) 10-fold magnified morphological image, obtained by averaging frames from a 5.6-second window; (b) manual definition of the aortic lumen, from which the radius vector, the mean aortic radius ($\overline{R}$), and the aortic centroid, (x_o, y_o), are calculated; (c) a cropped image. The position and dimension of the cropped region are automatically calculated based on $\overline{R}$ and (x_o, y_o).

D. Image segmentation

A flow diagram of the entire segmentation process is shown in Fig. 2. Each step is described next.

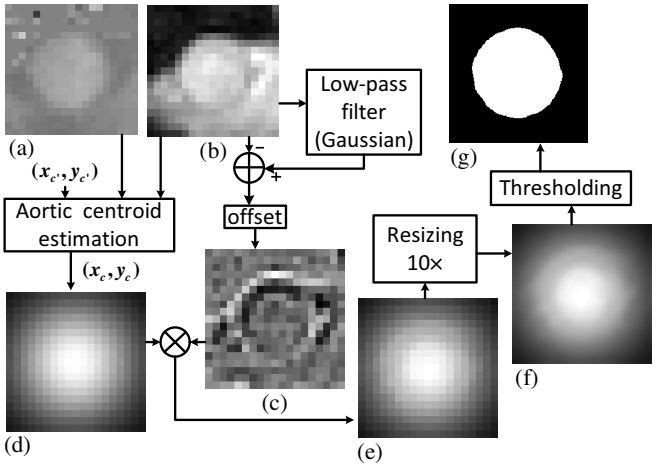

Fig. 2. Block diagram of the proposed segmentation algorithm.

1) Automatic tracking of the aortic centroid: The iterative process for tracking the aortic centroid is illustrated in Fig. 3. The algorithm starts by centering two ellipsoidal template images — whose radii and eccentricity are defined as shown in Fig. 1b — at the current centroid, (x_n, y_n). For the first iteration within a frame, (x_n, y_n) is set to $(x_{c'}, y_{c'})$, the estimated centroid for the previous frame. For the first iteration of the first frame, (x_n, y_n) is set to the manually defined centroid, (x_o, y_o).

Template I (Fig. 3a) is a two-dimensional combination of Gaussians, and highlights the aortic lumen in a low-pass image, obtained using unsharp masking after Gaussian filtering (Fig. 3b). This low-pass image is pixel-wise multiplied by Template I, and the resulting image is binarized, using a threshold level of 60% of its maximum amplitude.

Template II (Fig. 3c) is also a combination of two Gaussians, and highlights the aortic contour in a high-pass version of the cropped image, obtained using a Laplacian of Gaussian (LoG) filter (Fig. 3d). The high-pass image is pixel-wise multiplied by Template II, and the resulting image

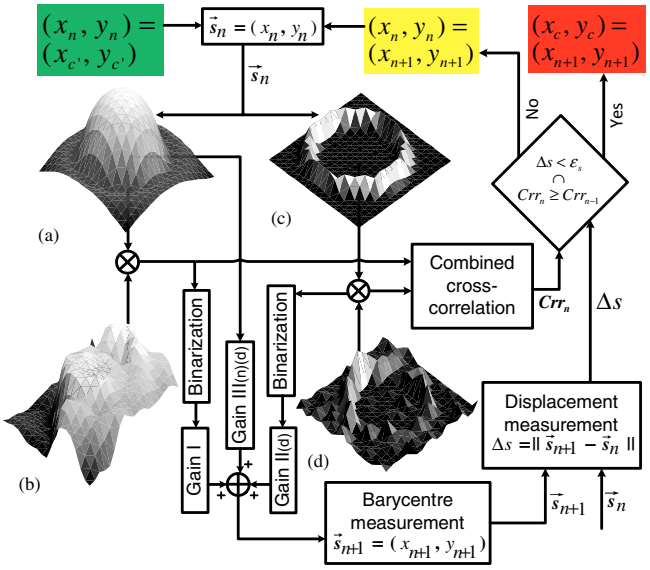

Fig. 3. Block diagram of the iterative algorithm for aortic centroid estimation.

is binarized at 10% of its maximum amplitude.

Template I and these two binarized images are combined using weighted averaging (examples of these combined images are shown in Fig. 4). Gain I — associated with the low-pass-based binary image — performs a coarse adjustment. Gain $\text{II}_{(d)}$ — associated with the high-pass-based binary image — performs fine adjustment, and is proportional to the standard deviation (d) of the cropped image. Gain $\text{III}_{(n)(d)}$ — associated with Template I — controls the displacement amplitude, and is proportional to the iteration number, n (this makes the process begin with a coarse adjustment, followed by a fine adjustment), and to the standard deviation, d (this makes the processs perform fewer iterations for low contrast images). The relationship between the variation in pixel intensities along the cardiac cycle and the construction of the barycenter image is illustrated in Fig. 5.

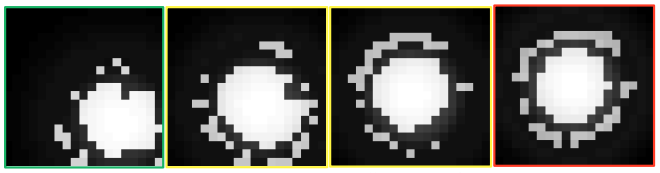

Fig. 4. A 10-iteration example of the iterative aortic centroid tracking process. Barycenter images obtained in iterations (i), (iv), (vii), and (x) are shown. The displacement (Δs) and the normalized (by the last value) combined cross-correlation (Crr) for each frame are indicated.

The barycentre displacement Δs from position s_n to position $\vec{s}_{n+1}$ is then calculated, and $\vec{s}_{n+1} = (x_{n+1}, y_{n+1}) = \left(\sum_{i=1}^{a}\sum_{j=1}^{b}(i.B[i,j], j.B[i,j])\right) / \left(\sum_{i=1}^{a}\sum_{j=1}^{b}(B[i,j])\right)$. If Δs is larger than a minimum displacement value ε_s, the center of the templates, $\vec{s}_n$, is updated to $\vec{s}_{(n+1)}$. The value of ε_s ranges from 1% and 10% of the prescribed radius $\overline{R}$, according to

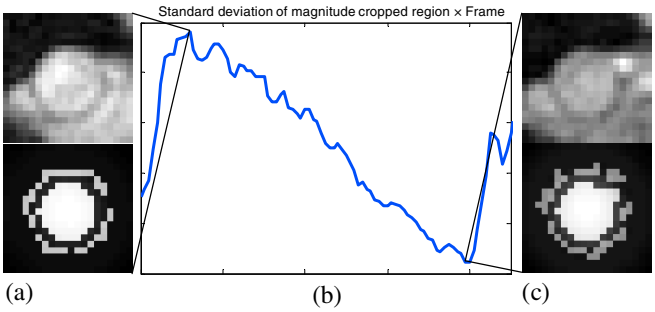

Fig. 5. Relationship between the variation in pixel intensities along the cardiac cycle (b) and the construction of the barycenter image. Morphological and barycenter images associated with (a) peak flow (highest standard deviation), and (c) end diastole (lowest standard deviaton) are shown. Note the difference in contour weight and definition in the barycenter images.

image quality (which is manually prescribed for the dataset, after visual inspection).

The centroid tracking process stops when Δs is smaller than ε_s. This is the point of maximum equilibrium, where the barycentre of $B[i,j]$ is an approximation of the centroid of the aorta. Hence, $\vec{s}_{(n+1)}$ is used to update our estimate of the aortic centroid, (x_c, y_c). An adjustment based on similarity is performed if Crr_n, the combined cross-correlation (a geometric mean of correlations) for the iteration is bigger than the combined cross-correlation for the previous iteration, Crr_{n-1}.

2) Segmentation based on a model image: Final segmentation is actually performed on a "model image", obtained based on a high-pass version of the original image. This may not provide the most millimetrically-accurate segmentation of the wall–lumen interface, but is robust in successfully separating aortic flow from neighboring flows. This is sufficient for calculating the aortic flow, which is the end-goal of this work.

This model image (Fig. 2e) is obtained by pixel-wise multiplication of: i) an offset high-pass image (Fig. 2c), obtained by subtracting a low-pass Gaussian-filtered image from the original image (Fig. 2b), where the offset level controls the shape of the segmented region (Fig. 6) (from perfectly round to very-closely following the contour of the high-pass image); and ii) a two-dimensional Gaussian, $G(x,y)$, centered at the estimated aortic centroid, (x_c, y_c) (Fig. 2d). The radius of this Gaussian is defined by the $\overline{R}$ value calculated during preprocessing, as follows:

$$G(x,y) = e^{-\left[(x-x_c)^2+(y-y_c)^2\right]/2\overline{R}^2}. \qquad (1)$$

The model image is magnified by 10-fold using bicubic interpolation, normalized to the [0,1] interval, and then segmented by thresholding (i.e., binarization). The threshold level $L = e^{-1/2} = 0.61$ is associated with the point where $(x-x_c)^2+(y-y_c)^2 = \overline{R}^2$, i.e., the point where $G(x,y) = 0.61$.

The use of the threshold level $L = 0.61$, applied to all images, assumes that the model image is the Gaussian itself. Thus, it provides a binary mask (Fig. 2g), whose format is close to a circle with radius $\overline{R}$. In order to avoid small errors in flow estimation due to radius variations associated with

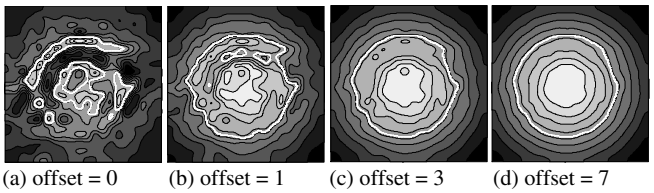

Fig. 6. The offset determines the smoothness of the segmentation from a: (a) not connected region to a; (d) to a region with great similarity with the aortic shape. Bigger offsets provide perfect circular regions

vessel dilatation and contraction during systole and diastole, respectively, the radius $\overline{R}$ is adaptively adjusted, based on the total flow in the cropped region of the velocity map from each frame. The curve of total cropped region flow (Fig. 7) is closely related to the actual aortic flow curve. Therefore, we assume that such curve also reflects aortic dilatation and contraction, i.e.: the higher the total flow, the larger the segmented radius should be. Therefore, we used this total flow information to adjust $\overline{R}$, and, hence, adjust the segmented area along the cardiac cycle. This adjustment factor is linearly associated with the total flow, and does not exceed 2 mm.

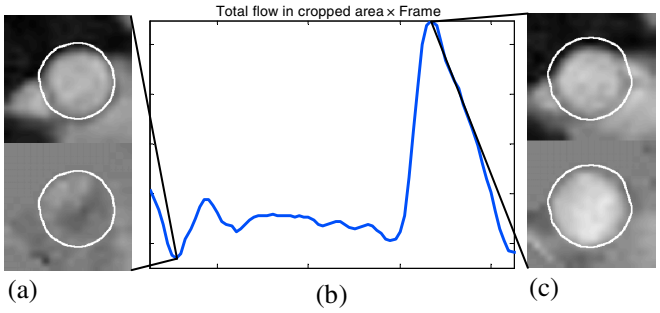

Fig. 7. Relationship between total flow at the cropped region along the cardiac cycle and aortic dilatation and contraction: (a) segmented image associated with the lowest total flow within a heartbeat (end diastole); (b) variation of total flow along one cardiac cycle; and (c) segmented image associated with the highest total flow within the same heartbeat (peak flow). Note the difference in aortic radii between images (a) and (c).

Using $L = 0.61$, we obtain a binary mask (Fig. 2g), which is the final goal of this paper. The measured velocities within this mask are averaged, and this average blood velocity is multiplied by the mask area, which results in the aortic flow associated with the current temporal frame. By integrating the flow waveform within each heartbeat, we estimate the stroke volume associated with each individual heartbeat.

III. Results

Due to the high temporal resolution requirements of flow measurement, and the use of real-time spiral MRI at 3 Tesla, all images display low resolution and low contrast. Still, the acquired datasets may be classified according to their image quality. Fig. 8 shows segmentation results for six temporal frames (covering systole) from three different subjects: one presenting reasonably good image quality (Fig. 8a); one presenting medium image quality (Fig. 8b); and one presenting

poor image quality (Fig. 8c). In all three cases, the proposed segmentation algorithm was able to track and isolate the aortic flow from neighboring flows, even though the interface between aortic wall and lumen is not visually well-defined.

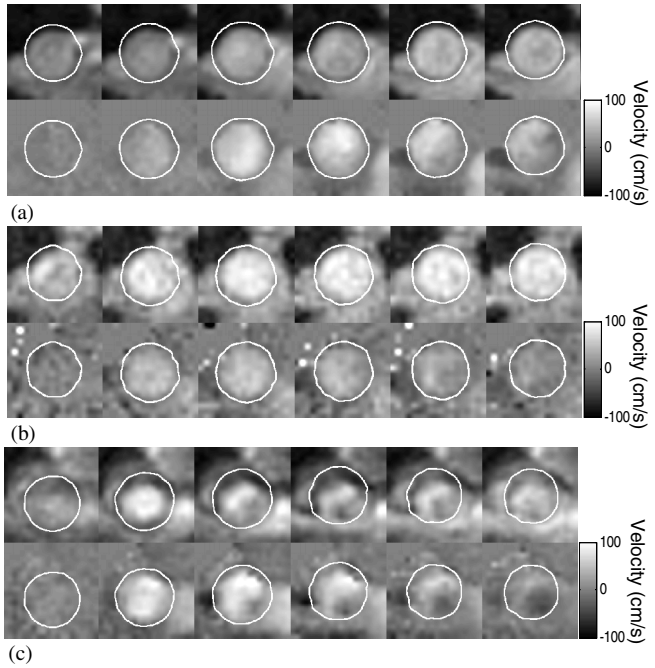

Fig. 8. Segmentation results for six temporal frames (covering systole) from three different subjects: (a) one presenting reasonably good image quality; (b) one presenting medium image quality; and (c) one presenting poor image quality.

Fig. 9a presents the flow waveform measured during five heartbeats from the subject in Fig. 8a. Similarly, Fig. 9b presents the flow waveform measured during one heartbeat from the subject in Fig. 8c. The smoothness of these curves illustrate how temporally-stable the algorithm is.

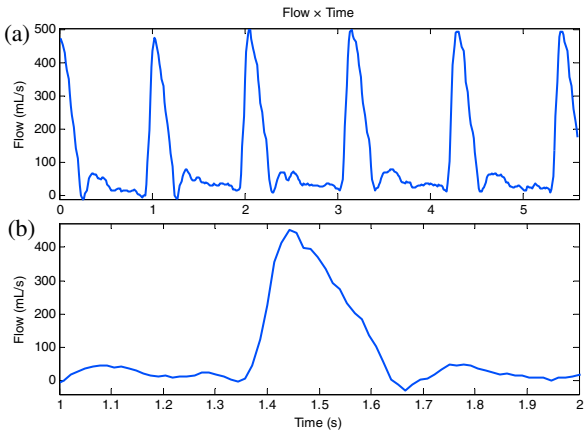

Fig. 9. Flow waveforms measured during (a) approximately five heartbeats from the subject in Fig. 8a; and (b) one heartbeat from the subject in Fig. 8c.

IV. Discussion

In our method, segmentation errors are typically caused by an overestimation or underestimation of the radius, or by inaccurate aortic centroid estimation. Slight overestimation of the aortic area does not incur in flow estimation errors, as long as the segmented region does not include significant flow external to the aorta. Slight underestimation of the aortic area may incur in flow estimation errors; however, this may not be significant, as aortic flow distant from the valve generally presents a parabolic profile. Pixels near the aortic wall — which would be neglected if there was underestimation of the aortic area — are very likely to present very low velocities, and, therefore, generally do not significantly contribute to the overall aortic flow. Assuming a parabolic profile, a 10% underestimation of the aortic radius or a 10% error in aortic centroid estimation would result in less than 4% error in flow estimation.

V. Conclusions

We presented a new model-based method for segmenting aortic flow in real-time spiral MRI images acquired at 3 Tesla. This allows more accurately measuring the stroke volume associated with each individual heartbeat, providing a non-invasive method for assessing stroke volume variability.

The proposed algorithm stands out from typical image segmentation methods by focusing on accurately separating the aortic flow from neighboring flows, instead of attempting to achieve a millimetrically-accurate segmentation of the interface between aortic wall and lumen. This provides robustness for measuring aortic flow, even when the interface between aortic wall and lumen is not visually distinguishable.

References

[1] V. Schekotov, M. Zubarev, O. Parandey, and A. Dumler, "Beat-to-beat variability of stroke volume output velocity measured by an impedance cardiographic method," in *13th International Conference on Electrical Bioimpedance and the 8th Conference on Electrical Impedance Tomography*. Springer, 2007, pp. 579–581.

[2] J. L. A. Carvalho, G. M. Pohos, and K. S. Nayak, "Stroke volume and cardiac output measured on a beat-to-beat basis," in *15th Scientific Meeting, International Society for Magnetic Resonance in Medicine*, Berlin, May 2007, p. 248.

[3] J. L. A. Carvalho, H. S Carvalho, and K. S. Nayak, "Measurement of beat-to-beat variability of stroke volume," in *11th SCMR*, 2008, p. 249.

[4] J. L. A. Carvalho, H. Carvalho, and K. Nayak, "Assessment of stroke volume variability using real-time spiral phase contrast," in *16th Scientific Meeting, International Society for Magnetic Resonance in Medicine*, 2008, p. 383.

[5] J. Steeden, D. Atkinson, A. Taylor, and V. Muthurangu, "Split-acquisition real-time cine phase-contrast mr flow measurements," *Magnetic Resonance in Medicine*, vol. 64, no. 6, pp. 1664–1670, 2010.

[6] A. Jones, J. Steeden, J. Pruessner, J. Deanfield, A. Taylor, and V. Muthurangu, "Detailed assessment of the hemodynamic response to psychosocial stress using real-time mri," *Journal of Magnetic Resonance Imaging*, vol. 33, no. 2, pp. 448–454, 2011.

[7] G. Kowalik, J. Steeden, B. Pandya, F. Odille, D. Atkinson, A. Taylor, and V. Muthurangu, "Real-time flow with fast gpu reconstruction for continuous assessment of cardiac output," *Journal of Magnetic Resonance Imaging*, 2012.

[8] M. Bernstein, K. King, and X. Zhou, *Handbook of MRI pulse sequences*. Academic Press, 2004.

[9] G.M. Gondim, and T.Z. Viana, Segmentation of the aorta in cardiac MRI sequences (in Portuguese),*B.S. thesis*, University of Brasilia, Braslia-DF, Brazil, 98 pages, 2008.

[10] D. Rueckert, P. Burger, S. Forbat, R. Mohiaddin, and G. Yang, "Automatic tracking of the aorta in cardiovascular mr images using deformable models," *Medical Imaging, IEEE Transactions on*, vol. 16, no. 5, pp. 581–590, 1997.